

Article

Effect of Precipitated Particles on Austenite Grain Growth of Al- and Nb-Microalloyed 20MnCr Gear Steel

Yingqi Zhu ¹, Shitao Fan ¹, Xiuzhen Lian ¹ and Na Min ^{1,2,*} 

¹ School of Materials Science and Engineering, Shanghai University, Shanghai 200444, China; zyq_@shu.edu.cn (Y.Z.); stfan@shu.edu.cn (S.F.); lianxiuzhen@shu.edu.cn (X.L.)

² Laboratory for Microstructures, Shanghai University, Shanghai 200444, China

* Correspondence: minnacy@shu.edu.cn

Abstract: The paper deals with the effect of the morphology characteristics, grain size, and the volume fraction of AlN- and NbC-precipitated particles on the prior austenite grain growth behavior in the Al- and Nb-microalloying 20MnCr gear steel during pseudo-carburizing heat treatments. The results indicate that the Nb addition in 20MnCr gear steel have a better effect on preventing austenite grain growth. The coarsening time after pseudo-carburizing in the Nb-microalloyed 20MnCr steel are improved by about 4 h compared with the Al-microalloyed steel. The precipitated particles coarsen and the number decreases with the pseudo-carburization temperature increasing, resulting in a reduction in the pinning pressure of the precipitated particles on the austenite grain boundaries. When the pseudo-carburization temperature reaches 1150 °C, the precipitated particles no longer have the ability to pin the austenite grain boundaries. In addition, the kinetics model for austenite grain growth under the process of the pinning and coarsening of the precipitated particles was established.

Keywords: microalloying; precipitated particles; austenite grain growth; pinning pressure



Citation: Zhu, Y.; Fan, S.; Lian, X.; Min, N. Effect of Precipitated Particles on Austenite Grain Growth of Al- and Nb-Microalloyed 20MnCr Gear Steel. *Metals* **2024**, *14*, 469. <https://doi.org/10.3390/met14040469>

Academic Editor: Babak Shalchi Amirkhiz

Received: 6 March 2024

Revised: 3 April 2024

Accepted: 13 April 2024

Published: 17 April 2024



Copyright: © 2024 by the authors. Licensee MDPI, Basel, Switzerland. This article is an open access article distributed under the terms and conditions of the Creative Commons Attribution (CC BY) license (<https://creativecommons.org/licenses/by/4.0/>).

1. Introduction

Gear steel is one of the most important materials for producing gears that meet performance requirements, among which 20MnCr gear steel is widely used due to its excellent mechanical properties and rich resources [1,2]. Gear steel has to undergo carburizing treatment because of its harsh working environment. After carburization, the surface of gear steel obtains a higher hardness, wear resistance, and fatigue strength, and the core part has a good toughness. But the conventional carburizing treatment always needs a long time to be carried out [3–7]. According to the Harris equation [8], when obtaining the same largeness of the carburized layer, increasing the carburizing temperature can significantly shorten the time required for carburization.

High-temperature carburization for gears is becoming more and more attractive in the past years because it can remarkably shorten the processing time, improve the production efficiency of the gear steel carburizing process, and reduce production costs [9–12]. However, the heating temperature has a significant impact on the grain growth of austenite; thus, prior austenite grains growing abnormally will reduce the properties of the materials [13–16].

It is well-known that grain growth is the microstructure evolution caused by the grain boundary movement driven by the decrease in the grain boundary interfacial energy [17]. At present, the most effective method to control grain growth is microalloying in steels. Controlling grain growth in microalloyed steels during high-temperature carburizing treatment depends critically on the precipitated particles [18]. Nb and Al microalloying have been regarded as effective ways to develop gear steel for high-temperature carburizing [19]. R.S. Varanasi et al. [20] presented that Nb microalloying hinders nucleation and austenite growth, reduces the austenite phase fraction, and, thus, greatly reduces plasticity. Genki

et al. [21] presented that nano-scale AlN- and Nb(C,N)-precipitated particles are mainly formed in the case-hardened steel of 35Al-32Nb (0.035 wt% Al, 0.032 wt% Nb), which exerts a significant pinning force on the austenite grain boundaries to prevent abnormal grain growth. M. Sennour et al. [22] presented that two types of AlN-precipitated particles have been found in low-carbon steel—cubic NaCl-type precipitates with a thin sheet shape and hexagonal precipitates with a coarse cubic shape—while the AlN precipitates in steels will dissolve if the carburizing temperature reaches up to 1000 °C [23]. Previous studies have demonstrated that the precipitation has a hindering effect on austenite grains during carburization. But there is currently no complete research providing basic data to analyze the effect of precipitates' characteristics on the grain growth of austenite during the high-temperature carburization process. Thus, by appreciating the characteristics of AlN- and NbC-precipitated particles, the effect of AlN- and NbC-precipitated particles on the grain growth of austenite can be understood.

In this study, the growth behavior of austenite grains and the microstructure characterization of the precipitated particles in the Al- and Nb-microalloying 20MnCr during pseudo high-temperature carburization has been investigated to understand the impact of the precipitated particles on austenite grain growth.

2. Materials and Methods

The steel 20MnCr with Al and Nb microalloying was used in this work. By using a SPECTRO MAXx (LMX16) direct-reading spectrometer (SPECTRO MAXx, Kleve, Germany), the chemical compositions of the investigated steels were determined, as provided in Table 1.

Table 1. Chemical composition of the investigated steels (main alloying elements, Wt.%).

Steel	C	Cr	Mn	Cr	Nb	Al	N	Fe
C0	0.20	0.23	1.41	1.15	-	0.03	0.02	Bal.
C1	0.25	0.25	0.71	1.12	0.200	-	0.01	Bal.

Cube specimens ($10 \times 10 \times 15 \text{ mm}^3$) were machined from the initial steel. The cube specimens were normalized at 875 °C for 35 min, and then air cooled to eliminate the impact of stress on subsequent tests. In order to reveal the prior austenite and obtain the average size of austenite grain, pseudo-carburizing needs be performed, which is to hold the samples at different austenitizing temperatures (950, 1050, and 1150 °C) for different times (0.5, 1, and 5 h), without carbon potential in the heat treatment furnace (Nabertherm 30-3000, Anklam, Germany), followed by water quenching. Figure 1 shows the schematic of the heat treatment process.

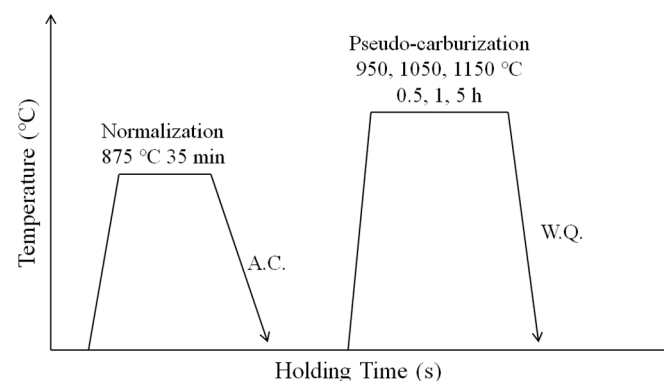


Figure 1. The schematic of the heat treatment process.

To observe the prior austenite grain boundary, the samples were etched for 3 min in a saturated aqueous solution of picric acid at 65 °C after being ground and polished using

conventional metallographic techniques. Microstructural observations were conducted on a Nikon EPIPHOT 300 optical microscopy (OM, Nikon EPIPHOT 300, Tokyo, Japan). Measure the average size of the prior austenite grain using the linear intercept method, and at least five fields of view were considered for each sample, with each field having 50–100 intercepts.

The morphology and distribution of the precipitated particles were observed on a ZEISS SUPRA 40 scanning electron microscope (SEM, ZEISS SUPRA 40, Kleve, Germany) operating at an accelerating voltage of 15 kV. In order to obtain the distribution of the precipitated particles, the SEM samples were also etched in the saturated picric acid aqueous solution.

The characteristics of precipitated particles were examined by a JEOL F200 transmission electron microscope (TEM, JEOL F200, Tokyo, Japan) equipped with energy-dispersive spectroscopy (EDS), which was used for TEM investigation at 200 kV. The distribution of the precipitated particles was obtained by the carbon extraction replica technique. The carbon replicas were prepared using LEICA EM ACE-600 high vacuum ion sputtering coating instrument (LEICA EM ACE-600, Kleve, Germany) after etching the samples with a 4% nitric acid alcohol solution. The thickness of the carbon layer is 20 nm.

To obtain the average size of the precipitated particles and analyze the size distribution, image analysis software (Image Pro Plus 6.0, MEDIA CYBERNETICS, Silver Spring, MD, USA) was used to measure the diameter of spherical precipitated particles and the side length of rod-shape precipitated particles. For the same sample, more than 200 precipitated particles were counted.

3. Results and Discussion

3.1. Evolution of Prior Austenite Grain Size with Temperature and Time

Figures 2–7 display the optical micrographs of the samples after being pseudo-carburized at 950 °C, 1050 °C, and 1150 °C for 0.5 h, 1 h, and 5 h, which show that the average grain size of the prior austenite gradually grows with the temperature increasing. At 950 °C, the mean size of the prior austenite grains (PAGs) in the C0 steel is 11.6 µm (Figures 2a, 3a and 4a), a little larger than that in the C1 steel (11.0 µm) (Figures 5a, 6a and 7a). And the PAGs are closed to the homogeneous microstructure. Abnormal grain growth can be observed at 1050 °C in the C0 steel, and the amount of the abnormally grown PAGs decreases with the time increasing, indicating the fine grains coarsen with the time being prolonged. At 1050 °C, normal coarsening grains occurred in C1 steel after being pseudo-carburized for 5 h, and the mean size of the PAGs is 38.7 µm, much larger than those for 0.5 h and 1 h. In addition, abnormal grain growth can be observed at 1150 °C in C1 steel. The results indicate that coarsening temperatures of the two steels after pseudo-carburizing for 0.5 h, 1 h, and 5 h are the same, but the coarsening time improved by about 4 h in C1 steel. Similarly, the average grain size is obviously reduced in C1 steel.

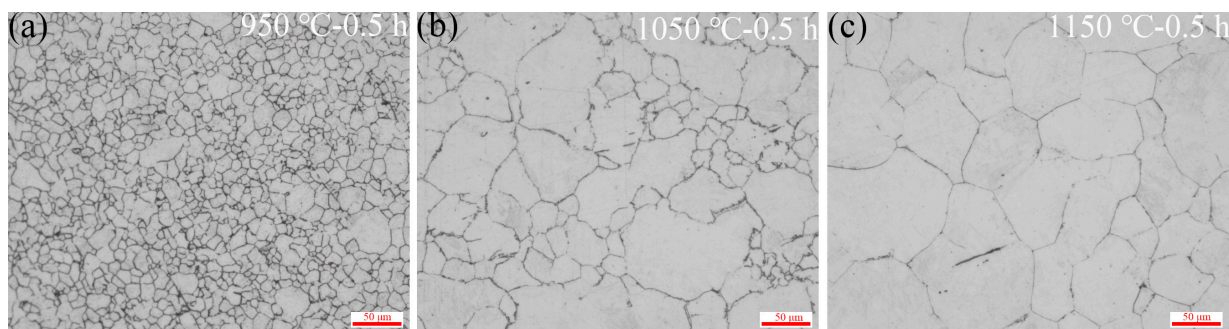


Figure 2. Optical micrographs of prior austenite grain in the C0 steel after pseudo-carburization at different temperature for 0.5 h: (a) 950 °C; (b) 1050 °C; and (c) 1150 °C.

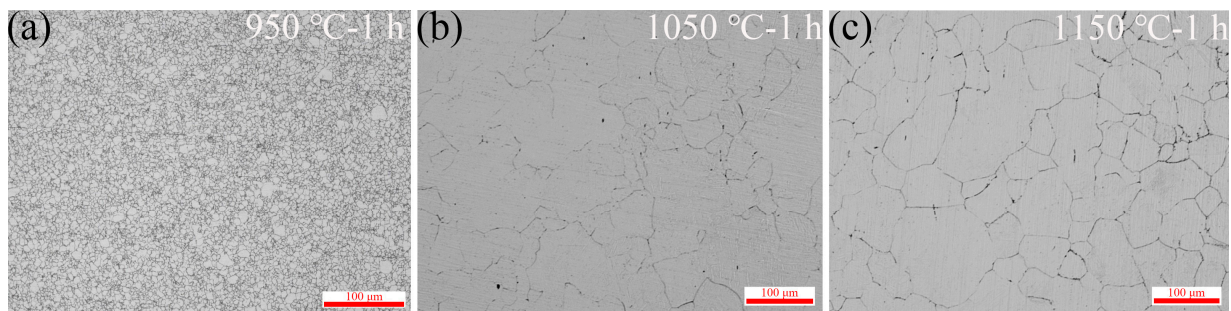


Figure 3. Optical micrographs of prior austenite grain in the C0 steel after pseudo-carburization at different temperature for 1 h: (a) 950 °C; (b) 1050 °C; and (c) 1150 °C.

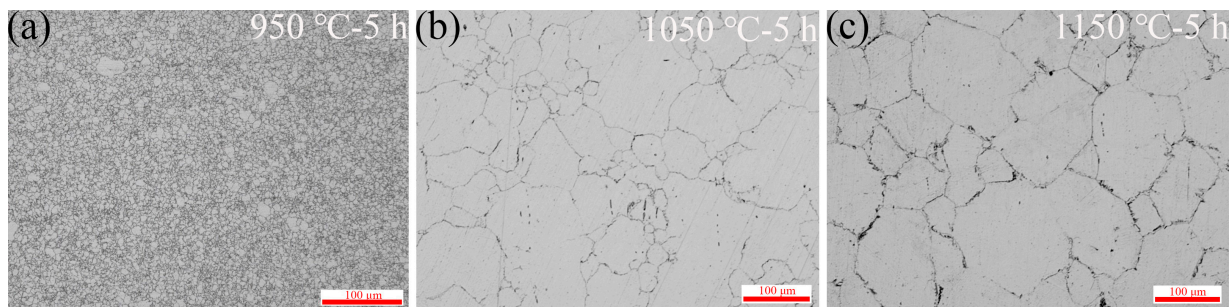


Figure 4. Optical micrographs of prior austenite grain in the C0 steel after pseudo-carburization at different temperature for 5 h: (a) 950 °C; (b) 1050 °C; and (c) 1150 °C.

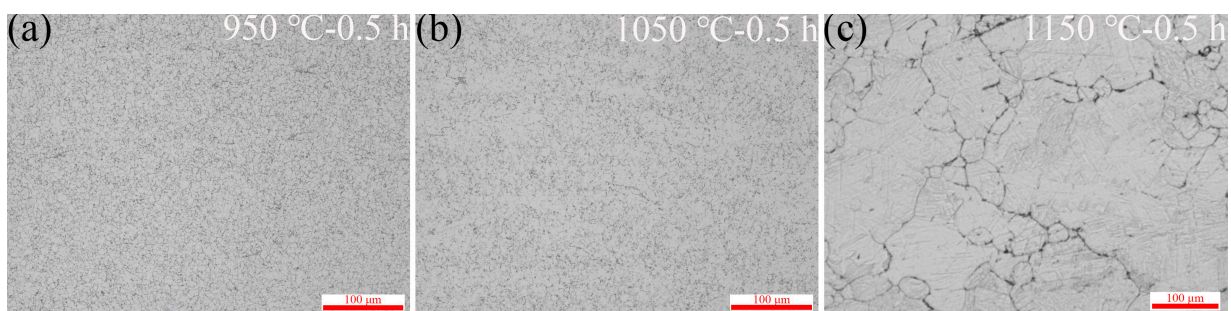


Figure 5. Optical micrographs of prior austenite grain in the C1 steel after pseudo-carburization at different temperature for 0.5 h: (a) 950 °C; (b) 1050 °C; and (c) 1150 °C.

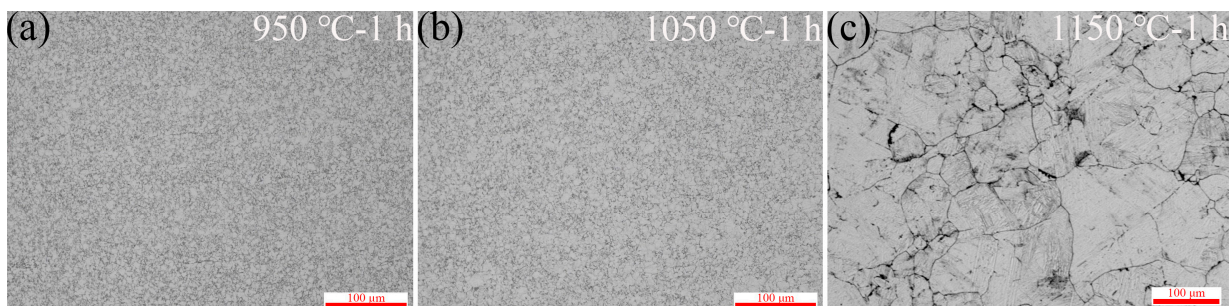


Figure 6. Optical micrographs of prior austenite grain in the C1 steel after pseudo-carburization at different temperature for 1 h: (a) 950 °C; (b) 1050 °C; and (c) 1150 °C.

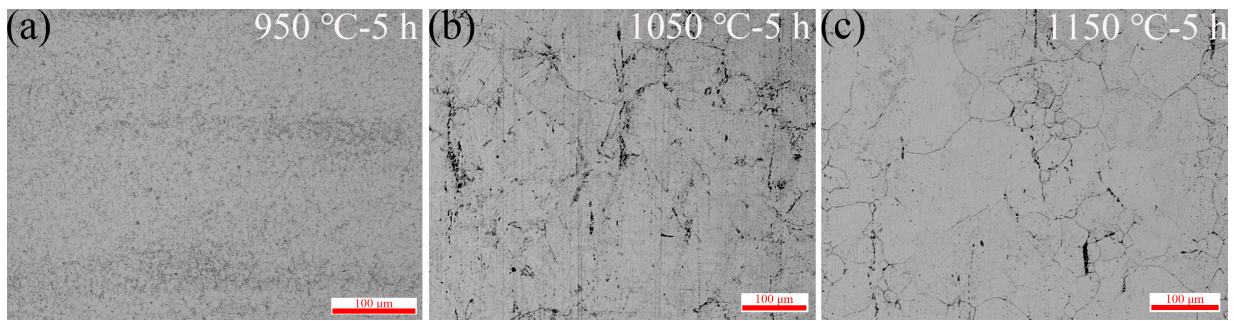


Figure 7. Optical micrographs of prior austenite grain in the C1 steel after pseudo-carburization at different temperature for 5 h: (a) 950 °C; (b) 1050 °C; and (c) 1150 °C.

Figure 8 shows the evolution of prior austenite grain size with temperature and time in the two steels. It is clear that the mean sizes of the PAGs in the C1 steel are smaller than those in the C0 steel under the same heat treatment. In addition, it can be found that the temperature of the heating treatment has a greater impact on the growth of the PAGs in the two steels. The growth rates of the grain size are relatively higher with the increase in temperature (Figure 8a,c) than those with the increase in time (Figure 8b,d). Moreover, the grain size of C0 steel increases linearly with the temperature, while the grain growth rate in the C1 steel is slow first, and fast afterwards. To sum up, the C1 steel has a better performance in the resistance to coarsening under high-temperature heat treatment compared to the C0 steel. It is also suggested that the different precipitated particles which exist in the matrix in the two steels will lead to the difference in the growth patterns of the PAGs. The effect of the characteristics of the precipitated particles on the growth of austenite grains deserves further research.

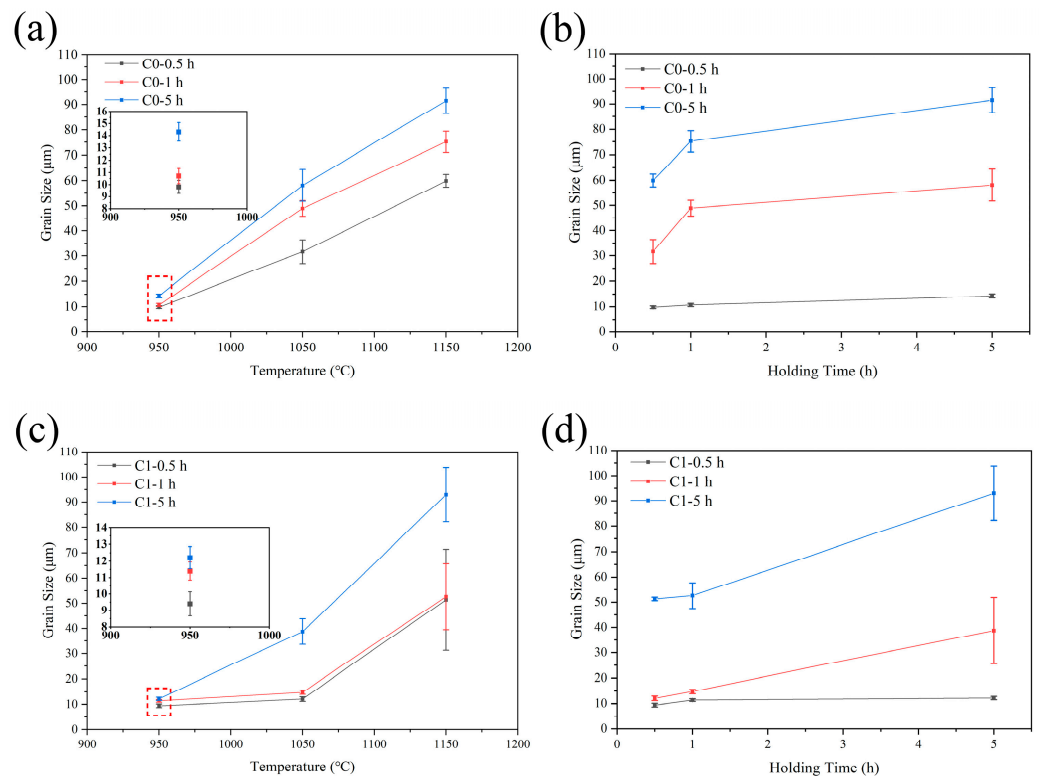


Figure 8. Grain size of prior austenite grain in different (a,c) temperatures and (b,d) times.

3.2. The Evolution of the Precipitated Particles

The precipitated particles play an important role in preventing grain boundary migration. The microalloying elements can form stable carbides and carbonitrides, which pin the austenite grains' boundary, with carbon and nitrogen in steel and disperse the carbides [24]. In order to obtain the microstructure characteristics of the precipitated particles in the two steels, TEM and SEM observations were conducted on the typical precipitated particles. Figure 9 exhibits the representative morphology of the precipitated particles in the C0 steel after pseudo-carburization at 950 °C for 0.5 h, and it can be observed that the precipitated particles are rod-shaped and have a size of micrometers. It is well-known that aluminum nitride is the most common precipitate in Al-addition gear steel. Combined with the results of selected-area electron diffraction (SAED) (Figure 9b) and the energy spectrum analysis (EDS) (Figure 9c) through spot scanning, it is obvious that the precipitated particle in the C0 steel is aluminum nitride. Meanwhile, the representative precipitated particles in the C1 steel pseudo-carburized at 1050 °C for 0.5 h are exhibited in Figure 10. The precipitated particles are spherical-shape, and located near the grain boundaries and within the grains. Through a more detailed observation by TEM, it is found that there are many nano-scale precipitated particles in the matrix that are not found by the SEM observation. In addition, the result of the EDS of the typical precipitated particles through spot scanning is shown in Figure 11c. By the SAED results, the precipitated particles have face-centered cubic structures, and then are identified as face-centered cubic structures NbC. Almost no coarsened NbC-precipitated particles were observed in the C1 steel after pseudo-carburizing at 950 °C for 1 h and 1050 °C for 1 h. In addition, the number of the nano-scale NbC particles decreases with the increase in the pseudo-carburization temperature and time.

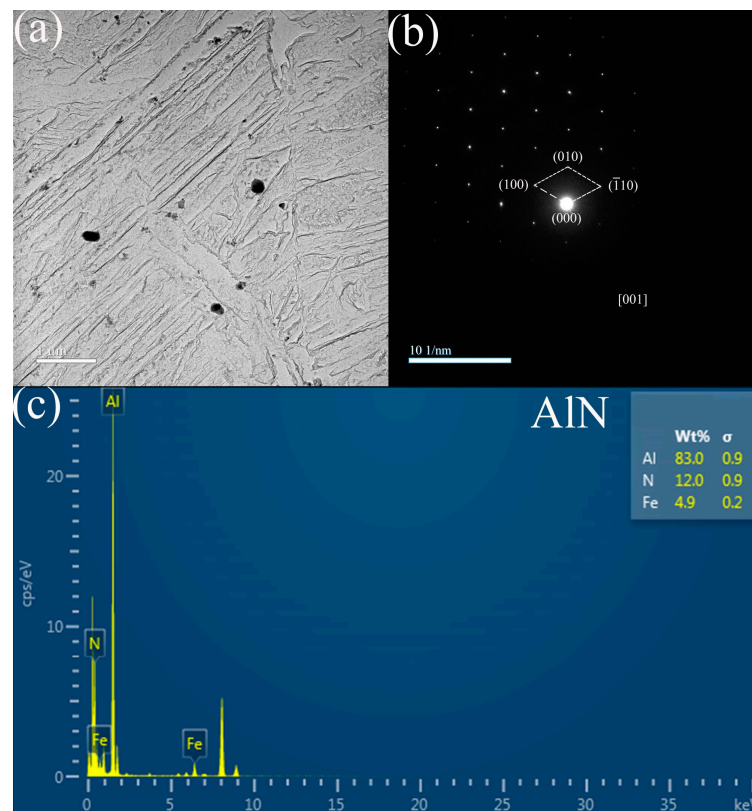


Figure 9. Determination of precipitated particles in the C0 steel after pseudo-carburization at 950 °C for 0.5 h: (a) TEM micrograph (BF), (b) corresponding selected area electron diffraction (SAED) pattern, and (c) EDS corresponding to the precipitated particle in (a).

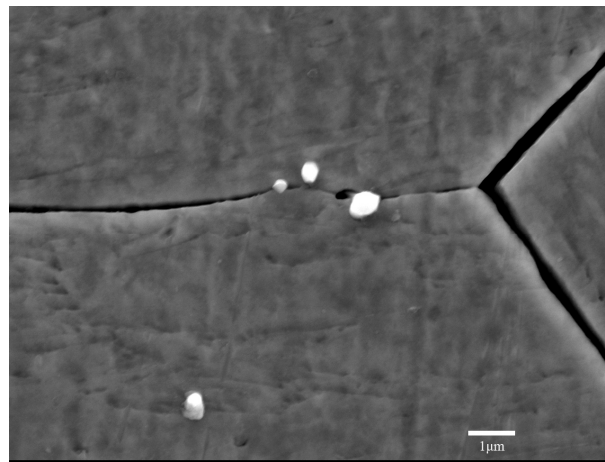


Figure 10. SEM micrograph of the precipitated particles in the C1 steel after pseudo-carburization at 1150 °C for 0.5 h.

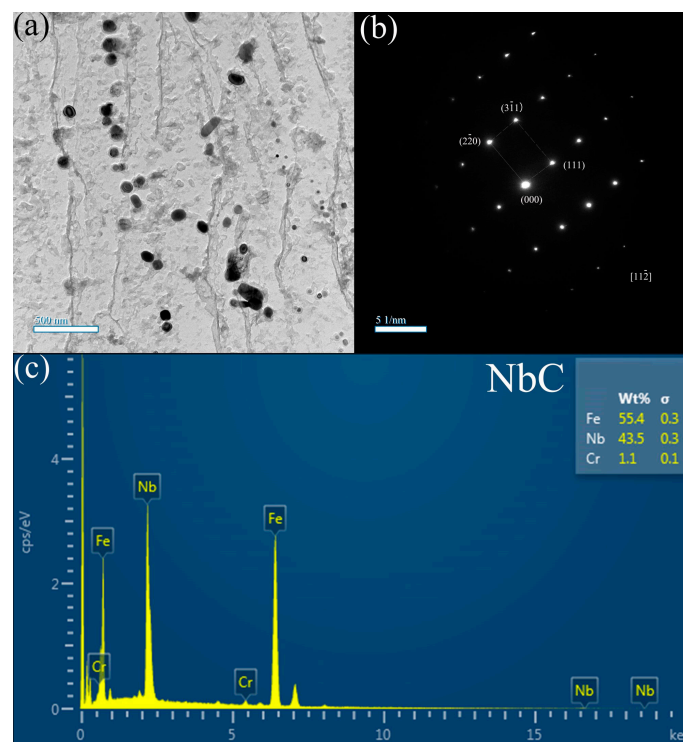


Figure 11. Determination of the precipitated particles in the C1 steel after pseudo-carburization at 1050 °C for 0.5 h: (a) TEM micrograph (BF), (b) NbC precipitate's SAED pattern, and (c) EDS corresponding to the precipitated particle in (a).

The precipitated particles grow or even dissolve with the temperature and holding time increasing, resulting in a weakening of the pinning effect on the austenite grains [25]. The solid solubility products of the AlN and NbC in austenite can be calculated using the following formulae, respectively [26]:

$$\log[\omega(\text{Al}) \times \omega(\text{N})]_{\gamma} = 1.95 - 7400/T \quad (1)$$

$$\log[\omega(\text{Nb}) \times \omega(\text{C})]_{\gamma} = 2.96 - 7510/T \quad (2)$$

where $\omega(X)$ is the mass fraction of element X, and T is the temperature of the solid solution. By calculation, the solid solution temperatures of AlN and NbC are 1158 °C and 1043 °C, respectively. However, previous studies [27] have shown that AlN-precipitated particles

will start dissolving back into the matrix at temperatures above 950 °C. When the temperature reaches 1000 °C, almost all AlN-precipitated particles dissolve, which lead to a loss of its pinning pressure on the austenite grain boundaries. Based on the TEM results of the steels after different heat treatments, the AlN-precipitated particles still exist at 1150 °C, but only a low amount of them can be observed, whereas the NbC-precipitated particles can be observed and their size undergoes substantial changes with the temperature and time increasing.

The size of the spherical NbC-precipitated particles can be obtained by measuring their diameter, and the grain size of the rod-shaped AlN-precipitated particles is measured by calculating the equivalent circular radius (r) using the following equation:

$$r = \sqrt{\frac{L_A L_B}{\pi}} \quad (3)$$

where L_A and L_B are the measured edge sizes of the AlN-precipitated particles. The size statistics of the NbC-precipitated particles in the C1 steel are shown in Figure 12. It is clear that the average diameter of the NbC-precipitated particles also increases with the temperature and holding time increasing. After holding for 0.5 h and 1 h at 950 and 1050 °C, the average diameters of the NbC particles are small, and few number of large NbC particles can be found. Nevertheless, as the holding time is prolonged, the peak of the grain size distribution of the precipitated particles gradually shifts to the right. The coarsening NbC particles play a more crucial role with the pseudo-carburization time prolonging. At 1150 °C, the size of most of the precipitated particles after being held for 0.5 h and 1 h is 100 nm and 140 nm, respectively. When the holding time is prolonged to 5 h, the size distribution tends to be equal. With a decrease in small-sized precipitated particles and an increase in large-sized precipitates, the size of the precipitated particles is inclined to increase to an average size. Moreover, the increase in the average grain size of the precipitated particles is also greatly influenced by the pseudo-carburization temperature. When the holding time is 0.5 h and the temperature increases from 950 °C to 1150 °C, the average grain size of NbC increases from 13.49 nm to 128.07 nm.

The area density fraction of the precipitated particles also plays a crucial role in inhibiting the austenite grain growth. The quantification of the area density fraction of carbide particles in the C1 steel can be obtained by calculating the volume fraction (f) of the precipitated particles, which can be calculated by substituting the radius of the precipitated particles (r) into Equation (4) [28], as shown in Figure 13:

$$f = \frac{N \frac{4\pi}{3} r^3}{SD} \quad (4)$$

where N is the number of precipitated particles in the selected area, S is the value of the selected area, and D is the equivalent diameter of the precipitated particles. It can be found that, when the holding time is 0.5 h and 1 h, although the grain size of the precipitated particles increases, the volume fraction decreases as the temperature and time increase. The reduction of the nano-scale carbide particles shows that some nano-scale carbide precipitated particles have dissolved during the pseudo-carburization treatment. Thus, it indicated that the NbC-precipitated particles in large quantities dissolve with the pseudo-carburization temperature and time increasing. Meanwhile, the dissolution of the NbC-precipitated particles gradually prospered with the pseudo-carburization temperature and time increasing. However, when the holding time is 5 h, the volume fraction increases or even exceeds the value when being held for 0.5 h. It demonstrated that, when the holding time is extended from 1 h to 5 h, the dissolution of the NbC-precipitated particles decreases or stops. However, there is a drastic decrease in the volume fraction of the NbC-precipitated particles which occurred in the C1 steel after pseudo-carburization at 1050 °C for 5 h. At this point, the PAGs in the C1 steel undergo coarsening. The drastic decrease in the volume fraction may be the main reason for the growth of the PAGs in the C1 steel.

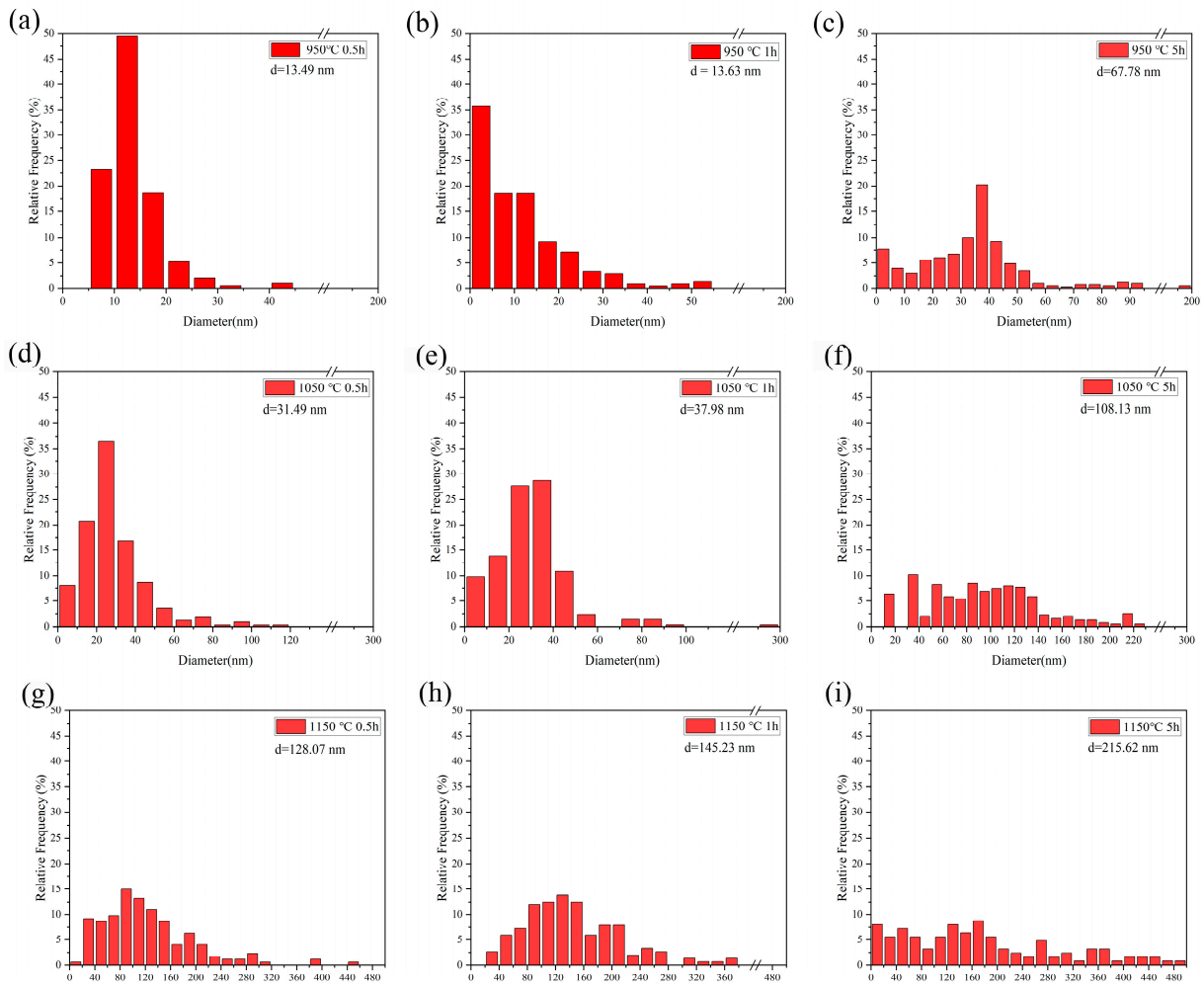


Figure 12. The size distribution of the NbC-precipitated particles in the C1 steel after pseudo-carburization at different temperatures for different times. The height of bars represents probability density (frequency). (a) at 950 °C for 0.5 h; (b) at 950 °C for 1 h; (c) at 950 °C for 5 h; (d) at 1050 °C for 0.5 h; (e) at 1050 °C for 1 h; (f) at 1050 °C for 5 h; (g) at 1150 °C for 0.5 h; (h) at 1150 °C for 1 h; (i) at 1150 °C for 5 h.

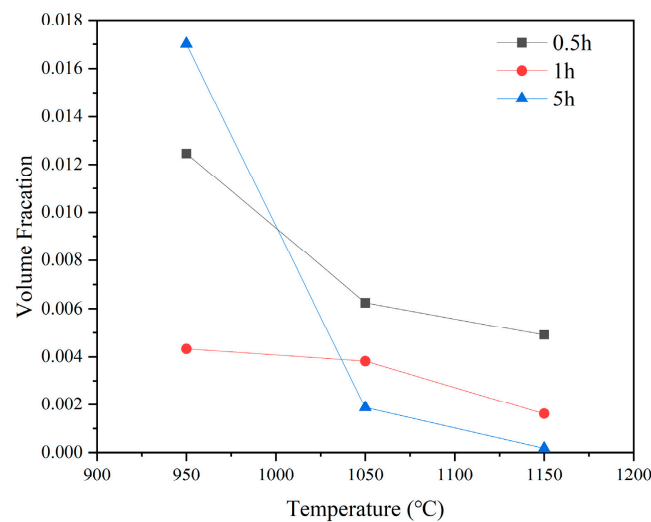


Figure 13. The volume fractions of the NbC-precipitated particles in the C1 steel.

In terms of the AlN-precipitated particles, the average diameter of the AlN-precipitated particles after pseudo-carburization for 0.5 h at 950 °C is 187.38 nm (Figure 14), which is much larger than the NbC-precipitated particles in the C1 steel. Moreover, the volume fraction of the AlN-precipitated particles is 1.42×10^{-3} . By calculating its pinning pressure, it is suggested that it has no ability to pin austenite grain boundaries. This causes the PAGs in the C0 steel to coarsen at 1050 °C. Thus, it is confirmed that the C1 steel (Nb-microalloyed steel) possesses both finer precipitated particles and a higher density of precipitated particles at high temperatures, which can better solve the problem of abnormal prior austenite growth during high-temperature carburization.

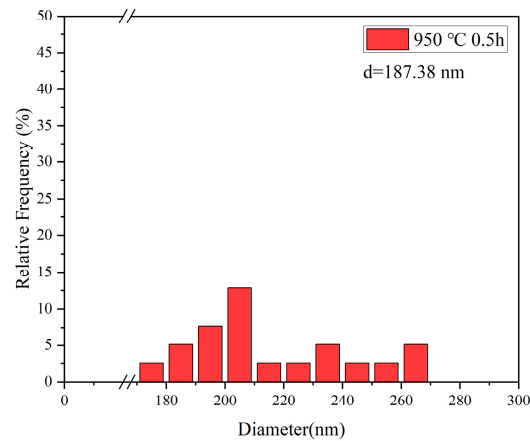


Figure 14. Size distribution of the AlN-precipitated particles in the C0 steel after pseudo-carburization at 950 °C for 0.5 h.

3.3. Effect of Precipitated Particles on Austenite Grain Size

The quantification of the effect of the precipitated particles on austenite grain growth can be obtained by calculating the pinning pressure. The pinning pressure (F_Z) is related to the volume fraction and average radius of the precipitated particles. By substituting f and r into the following equation [29], the pinning pressure can be obtained; the results are showed in Figure 15:

$$F_Z = \beta \frac{\gamma f}{r} \quad (5)$$

where β is a dimensionless constant assumed to be 12 [29], and γ is the interfacial energy of austenite.

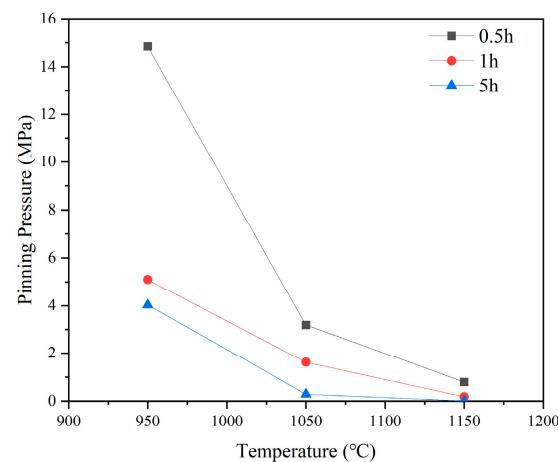


Figure 15. Pinning pressure of the NbC-precipitated particles in the C1 steel at different pseudo-carburizing treatments.

When the carbon content (C) in steel is lower than 0.8% (wt.%), γ can be calculated by the following equation [30]:

$$\gamma = (0.8 - 0.35C^{0.68}) \quad (6)$$

According to Equation (5), the interfacial energy of C1 steel is 0.67 J/m².

It can be found that the pinning pressure decreases with the temperature and holding time increasing. At 950 °C, the pinning pressure of the NbC-precipitated particles in the C1 steel held for 0.5 h reaches 14.84 MPa, which can effectively pin the austenite grain boundaries and hinder the austenite grain growth. As the holding time is prolonged, the pinning pressure decreases, reaching 5.10 MPa at 1 h and 4.03 MPa at 5 h, gradually losing its pinning effect on the grain boundaries. Consistent with the growth line of 950 °C, the pinning pressures at 1050 °C and 1150 °C decrease with the holding time increasing. However, the pinning pressures at 1150 °C held for 0.5 h and at 1050 °C held for 5 h are 0.79 MPa and 0.27 MPa, respectively, where the pinning effect on the grain boundaries is very slight.

3.4. Kinetics of Austenite Grain Growth during the Precipitated Particle Grow

At the same pseudo-carburizing temperature, as the holding time is prolonged, the austenite grains grow. The Beck equation [31] can be used to study the relationship between the average grain size of austenite (D) and the heat treatment holding time (t) under isothermal conditions:

$$D = Kt^n \quad (7)$$

where K is the rate of grain growth, n is the grain growth index, and K and n are constants related to the material and temperature.

By taking the logarithms on both sides of Equation (7), it can be obtained that:

$$\ln D = \ln K + n \ln t \quad (8)$$

The grain growth can be described as a straight line with the average grain size changing with the holding time (the horizontal axis is $\ln t$, and the vertical axis is $\ln D$), where n is the slope of the straight line and $\ln K$ is the intercept. The results of n and $\ln K$ are showed in Table 2. It can be observed that the slope of the fitted curve n first increases, and then decreases with the temperature increasing. It indicated that the growth of austenite is inhibited at 950 °C, but the growth rate of austenite grains in the C1 steel is very fast at 1050 °C where the precipitate particles lose their pinning pressure on the grain boundaries. When the temperature goes up to 1150 °C, austenite returns to its normal growth state.

Table 2. Results of austenite grain growth in Beck model in the C1 steel.

Grain Growth Index	950 °C	1050 °C	1150 °C
n	0.1	0.52	0.28
$\ln K$	1.53	−1.48	1.81

The driving pressure for the austenite grain growth is the grain boundary free energy (interfacial energy), but the existence of the precipitated particles can hinder grain growth. Considering the pinning pressure of the precipitated particles, the rate of grain growth K can be expressed by the Zener model [29]:

$$K = M(F_D - F_Z) \quad (9)$$

where M is the interface boundary mobility, F_D is the driving pressure of the precipitates, and F_Z is the pinning pressure of the precipitates. F_D can be calculated by:

$$F_D = \alpha \frac{\gamma}{D} \quad (10)$$

where α is a coefficient, the value of which is 4 [29], and D is the grain diameter.

The interface boundary mobility M can be described by the Arrhenius law [32]:

$$M = M_0 \exp\left(-\frac{Q}{RT}\right) \quad (11)$$

where M_0 is a pre-exponential factor; R is the gas constant, the value of which is 8.314 J/(mol·K); T is the temperature; and Q is the activation energy for grain boundary mobility.

Therefore, Equation (7) can be rewritten as:

$$D = M_0 \exp\left(-\frac{Q}{RT}\right) (F_D - F_Z) t^n \quad (12)$$

The model for austenite grain growth in the process of the growth and coarsening of the NbC-precipitated particles can be obtained by incorporating the values calculated above into Equation (12):

$$D_{\text{Nb}-\gamma} = 5.3 \exp\left(-\frac{166}{RT}\right) t^n \quad (13)$$

4. Conclusions

We investigated the effect of the morphology, the grain size, and the volume fraction of the AlN- and NbC-precipitated particles on the behavior of the grain growth of the prior austenite grain in the Al- and Nb-microalloying 20MnCr gear steel. The following conclusions can be drawn:

- (1) With the increase in the pseudo-carburization temperature, the precipitated particles AlN and NbC in the Al- and Nb-microalloying 20MnCr gear steel coarsen and the number density decreases. The grain-coarsening time after pseudo-carburizing at 950 °C, 1050 °C, and 1150 °C is improved by about 4 h in the C1 steel.
- (2) The pinning force of the NbC-precipitated particles to the austenite grain boundary decreases with the increasing in the pseudo-carburization temperature and holding time. At 950 °C for 0.5 h, the pinning force reaches the maximum, which can effectively pin the austenite grain boundaries. However, when the pseudo-carburization temperature reaches 1150 °C, the NbC-precipitated particles no longer have the ability to pin the austenite grain boundaries.
- (3) Based on the Beck model, the pinning effect of the NbC-precipitated particles was considered and the kinetics model for austenite grain growth in the process of the growth and coarsening of the precipitated particles was established:
 $D_{\text{Nb}-\gamma} = 5.3 \exp\left(-\frac{166}{RT}\right) t^n$.

Author Contributions: Conceptualization, Y.Z. and N.M.; methodology, Y.Z., S.F., X.L. and N.M.; software, Y.Z.; validation, N.M.; investigation, N.M.; resources, N.M.; data curation, Y.Z., S.F., X.L. and N.M.; writing—original draft preparation, Y.Z., S.F., X.L. and N.M.; writing—review and editing, N.M.; visualization, Y.Z.; supervision, N.M.; project administration, N.M.; funding acquisition, N.M. All authors have read and agreed to the published version of the manuscript.

Funding: This research was funded by the National Natural Science Foundation of China, grant number 52071209.

Data Availability Statement: The original contributions presented in the study are included in the article, further inquiries can be directed to the corresponding author.

Conflicts of Interest: The authors declare no conflicts of interest.

References

1. Wang, J.; Peng, J.; Zhang, F.; Li, Y.J.; Zhang, X.; An, S.L. Effects of Ce-Modified TiN Inclusions on the Fatigue Properties of Gear Steel 20CrMnTi. *Crystals* **2023**, *13*, 13071071. [[CrossRef](#)]
2. Miler, D.; Hoić, M. Optimisation of cylindrical gear pairs: A review. *Mech. Mach. Theory* **2021**, *156*, 104156. [[CrossRef](#)]
3. Xue, Y.J.; Yan, Y.M.; Yu, W.C.; Dong, M.Z.; Shi, J.; Wang, M.Q. Microstructure and fatigue properties of 17Cr2Ni2MoVNb gear steel after gas carburizing and low-pressure carburizing. *Int. J. Fatigue* **2023**, *167*, 107314. [[CrossRef](#)]
4. Yin, L.C.; Ma, X.X.; Tang, G.Z.; Fu, Z.Y.; Yang, S.X.; Wang, T.J.; Wang, L.Q.; Li, L.H. Characterization of carburized 14Cr14Co13Mo4 stainless steel by low pressure carburizing. *Surf. Coat. Technol.* **2019**, *358*, 654–660. [[CrossRef](#)]
5. O'Brien, E.C.H.C.; Yeddu, H.K. Multi-length scale modeling of carburization, martensitic microstructure evolution and fatigue properties of steel gears. *J. Mater. Sci. Technol.* **2020**, *49*, 157–165. [[CrossRef](#)]
6. Qin, S.W.; Zhang, C.H.; Zhang, B.; Ma, H.Y.; Zhao, M.H. Effect of carburizing process on high cycle fatigue behavior of 18CrNiMo7-6 steel. *J. Mater. Res. Technol.* **2022**, *16*, 1136–1149. [[CrossRef](#)]
7. Wang, B.; He, Y.P.; Liu, Y.; Tian, Y.; You, J.L.; Wang, Z.D.; Wang, G.D. Mechanism of the Microstructural Evolution of 18Cr2Ni4WA Steel during Vacuum Low-Pressure Carburizing Heat Treatment and Its Effect on Case Hardness. *Materials* **2020**, *13*, 13102352. [[CrossRef](#)]
8. Matlock, D.K.; Alogab, K.A.; Richards, M.D.; Speer, J.G. Surface Processing to Improve the Fatigue Resistance of Advanced Bar Steels for Automotive Applications. *Mater. Res.* **2005**, *8*, 453–459. [[CrossRef](#)]
9. Xue, Y.J.; Yan, Y.M.; Yu, W.C.; He, X.F.; Shi, J.; Wang, M.Q. Determination of solid solubility products of [Nb][C] in the case and the core of high-temperature carburizing steel by extraction phase analysis method. *Mater. Lett.* **2022**, *310*, 131519. [[CrossRef](#)]
10. Yuan, J.F.; Xiao, Y.; Min, N.; Li, W.; Zhao, S.X. The Influence of Precipitate Morphology on the Growth of Austenite Grain in Nb-Ti-Al Microalloyed Steels. *Materials* **2022**, *15*, 15093176. [[CrossRef](#)]
11. He, G.N.; Zhang, N.; Wan, S.Q.; Zhao, H.D.; Jiang, B.; Liu, Y.Z.; Wu, C.J. The Carburizing Behavior of High-Temperature Short-Time Carburizing Gear Steel: Effect of Nb Microalloying. *Steel Res. Int.* **2022**, *93*, 202200427. [[CrossRef](#)]
12. Kula, P.; Pietrasik, R.; Dybowski, K.; Paweta, S.; Wolowicz, E. Properties of Surface Layers Processed By a new, High-temperature Vacuum Carburizing Technology with PreNitriding-PreNitLPC. *Manag. Manuf. Mater. Eng.* **2012**, *452–453*, 401–406. [[CrossRef](#)]
13. Chen, R.C.; Hong, C.; Li, J.J.; Zheng, Z.Z.; Li, P.C. Austenite grain growth and grain size distribution in isothermal heat-treatment of 300M steel. *Int. Conf. Technol. Plast.* **2007**, *207*, 663–668. [[CrossRef](#)]
14. Chamanfar, A.; Chentouf, S.M.; Jahazi, M.; Lapiere-Boire, L.P. Austenite grain growth and hot deformation behavior in a medium carbon low alloy steel. *J. Mater. Res. Technol.* **2020**, *9*, 12102–12114. [[CrossRef](#)]
15. Hong, G.; Liu, H.S.; Dong, Y.N.; Zheng, H.G.; Xu, G.D.; Zhang, J.Q. Study on kinetics of austenite grain growth of micro-alloyed peritectic steels under high temperatures. *J. Iron Steel Res.* **2021**, *33*, 1270–1277.
16. Tang, E.; Yuan, Q.; Zhang, R.; Zhang, Z.C.; Mo, J.X.; Liang, W.; Xu, G. On the grain coarsening behavior of 20CrMnTi gear steel during pseudo carburizing: A comparison of Nb-Ti-Mo versus Ti-Mo microalloyed steel. *Mater. Charact.* **2023**, *203*, 113138. [[CrossRef](#)]
17. Wang, H.R.; Wang, W. Simple model for austenite grain growth in microalloyed steels. *Mater. Sci. Technol.* **2008**, *24*, 228–232. [[CrossRef](#)]
18. Fang, F.; Yong, Q.L.; Yang, C.F.; Su, H. A Model for Precipitation Kinetics in Vanadium Microalloyed Steel. *J. Iron Steel Res. Int.* **2010**, *17*, 36–42. [[CrossRef](#)]
19. Alogab, K.A.; Matlock, D.K.; Speer, J.G.; Kleebe, H.J. The influence of niobium microalloying on austenite grain coarsening behavior of Ti-modified SAE 8620 steel. *ISIJ Int.* **2007**, *47*, 307–316. [[CrossRef](#)]
20. Varanasi, R.S.; Gault, B.; Ponge, D. Effect of Nb micro-alloying on austenite nucleation and growth in a medium manganese steel during intercritical annealing. *Acta Mater.* **2022**, *229*, 117786. [[CrossRef](#)]
21. Saito, G.; Sakaguchi, N.; Ohno, M.; Matsuura, K.; Takeuchi, M.; Sano, T.; Minoguchi, K.; Yamaoka, T. Effects of Concentrations of Micro-alloying Elements and Hotforging Temperature on Austenite Grain Structure Formed during Carburization of Case-hardening Steel. *ISIJ Int.* **2020**, *60*, 2549–2557. [[CrossRef](#)]
22. Sennour, M.; Esnouf, C. Contribution of advanced microscopy techniques to nanoprecipitates characterization: Case of AlN precipitation in low-carbon steel. *Acta Mater.* **2003**, *51*, 943–957. [[CrossRef](#)]
23. Manabu, K.; Tatsuro, O. Development of High Strength Steels for Automobiles. *Nippon Steel Tech. Rep.* **2003**, *88*, 81.
24. Huang, S.G.; Vanmeensel, K.; Mohrbacher, H.; Woydt, M.; Vleugels, J. Microstructure and mechanical properties of NbC-matrix hardmetals with secondary carbide addition and different metal binders. *Int. J. Refract. Met. Hard Mater.* **2015**, *48*, 418–426. [[CrossRef](#)]
25. Zhang, Y.; Li, X.H.; Liu, Y.C.; Liu, C.X.; Dong, J.; Yu, L.M.; Li, H.J. Study of the kinetics of austenite grain growth by dynamic Ti-rich and Nb-rich carbonitride dissolution in HSLA steel: In-situ observation and modeling. *Acta Mater.* **2020**, *169*, 110612. [[CrossRef](#)]
26. Ainslie, N.G.; Hoffman, R.E.; Seybolt, A.U. Sulfur segregation at α -iron grain boundaries. *Acta Metallurgica* **1960**, *8*, 523–527. [[CrossRef](#)]
27. Kundu, A.; Davis, C.; Strangwood, M.; Brechet, Y.; Clouet, E.; Deschamps, A.; Finel, A.; Soisson, F. Pinning of Austenite Grain Boundaries by Mixed AlN and Nb(C,N) Precipitates. *Solid State Phenom.* **2011**, *172–174*, 458–463. [[CrossRef](#)]

28. Tian, D.W.; Karjalainen, L.P.; Qian, B.N.; Chen, X.F. Nonuniform distribution of carbonitride particles and its effect on prior austenite grain size in the simulated coarse-grained heat-affected zone of thermomechanical control-processed steels. *Metall. Mater. Trans. A-Phys. Metall.* **1996**, *27*, 4031–4038. [[CrossRef](#)]
29. Miodownik, M.A. Zener Pinning. In *Encyclopedia of Materials: Science and Technology*; Elsevier: Amsterdam, The Netherlands, 2001; pp. 9855–9859.
30. Militzer, M.; Giumelli, A.; Hawbolt, E.B.; Meadowcroft, T.R. Austenite grain growth kinetics in Al-killed plain carbon steels. *Metall. Mater. Trans. A Phys. Metall.* **1996**, *27*, 3399–3409. [[CrossRef](#)]
31. Beck, P.A.; Kremer, J.C.; Demer, L.J.; Holzworth, M.L. Grain growth in high-purity aluminum and in an aluminum-magnesium alloy. *Trans. Am. Inst. Min. Metall. Eng.* **1948**, *175*, 372–400.
32. Maalekian, M.; Radis, R.; Militzer, M.; Moreau, A.; Poole, W.J. In situ measurement and modelling of austenite grain growth in a Ti/Nb microalloyed steel. *Acta Mater.* **2012**, *60*, 1015–1026. [[CrossRef](#)]

Disclaimer/Publisher’s Note: The statements, opinions and data contained in all publications are solely those of the individual author(s) and contributor(s) and not of MDPI and/or the editor(s). MDPI and/or the editor(s) disclaim responsibility for any injury to people or property resulting from any ideas, methods, instructions or products referred to in the content.